

A new empirical method to estimate the molecular gas mass in galaxies.

Alice Concas,^{1,2,3*} Paola Popesso¹

¹*Excellence Cluster Universe, Boltzmannstr. 2 D-85748 Garching, Germany*

²*Cavendish Laboratory, University of Cambridge, 19 J. J. Thomson Ave., Cambridge CB3 0HE, UK*

³*Kavli Institute for Cosmology, University of Cambridge, Madingley Road, Cambridge CB3 0HA, UK*

Accepted XXX. Received YYY; in original form ZZZ

ABSTRACT

We find a tight correlation between the dust extinction, traced by the Balmer Decrement ($BD=H\alpha/H\beta$), the CO(1-0) line luminosity (L_{CO}) and total molecular gas mass (M_{H_2}) in a sample of 222 local star-forming galaxies drawn from the xCOLD GASS survey. As expected, the galaxy disk inclination affects the correlation by inducing a saturation of the Balmer decrement on highly inclined galaxies. Once this effect is taken into account, L_{CO} and M_{H_2} can be expressed as a function of BD with a scatter of ~ 0.3 dex. We do not find any dependence on galaxy size, mass, morphology, star formation activity and gas metallicity. The correlation disappears if the atomic gas phase is considered. This is likely due to the fact that the region traced by the BD, the stellar disk, is much smaller than the HI disk.

Key words: galaxies: ISM – ISM: dust, extinction – ISM: molecules

1 INTRODUCTION

The star formation activity of galaxies is governed by the complex relationship between gas and dust. While dust works as catalyst in transforming atomic hydrogen (HI) into molecular hydrogen (H₂), the collapse of giant molecular clouds leads to the star formation process itself (e.g., Wolfire et al. 1995). It is clear, then, that the molecular gas is the most accurate tracer of the star formation regions and it is essential to understand the details of the process.

The molecular phase gas is not directly observable (see Kennicutt & Evans 2012 for a review). Commonly the luminosity due to the $J=1-0$ transition of the carbon monoxide molecule (CO) is used as a good proxy of the H₂ gas mass (e.g. Kennicutt & Evans 2012; Bolatto 2015; Saintonge et al. 2011, 2017). However, despite the great potential of this method, CO observations are extremely time-consuming. Also in era of huge, new millimeter facilities, as the Atacama Large Millimeter/submillimeter Array (ALMA), building a statistically significant CO galaxy survey is still challenging.

A powerful alternative to estimate the molecular gas mass is the use of the well known empirical gas-to-dust mass relation (e.g Bourne et al. 2013; Scoville et al. 2014; Groves et al. 2015; Bertemes et al. 2018). The dust emission has been used to estimate gas content in the Milky Way (e.g., Dame et al. 2001), and in nearby galaxies by a number of authors (e.g., Israel et al. 1996; Israel 1997, 2005;

Leroy et al. 2009; Boquien et al. 2013a). In addition, it has been extended to sub-mm observations (James et al. 2002) and more recently to Herschel data (e.g., Eales et al. 2010, 2012; Roman-Duval et al. 2010). For instance, Scoville et al. (2014, 2015, 2016, 2017) apply a similar concept to the Rayleigh-Jeans side of the spectral energy distribution of local and high- z galaxies. The cold gas mass is estimated by converting the luminosity at rest frame of 850 μm into cold gas mass with a scaling relation calibrated on local and high redshift galaxies (see Scoville et al. 2016 for more details).

More recently, an alternative method has been proposed to retrieve the molecular gas mass based on the absorption rather than the emission of to the dust grains, (e.g. Brinchmann et al. 2013; Kreckel et al. 2013; Boquien et al. 2013b; Barrera-Ballesteros et al. 2018). Such methodologies are based on the fact that, in the HII regions, the young ionizing O stars are commonly associated with the clouds of cold gas from which they formed (Calzetti et al. 1994; Charlot & Fall 2000). Such surrounding dust is able to absorb the energetic photons leaving an imprint in the UV and optical light, and leading to a well known correlation between the dust column density and the reddening or the extinction of starlight (e.g. Kennicutt & Evans 2012; Kreckel et al. 2013). For this reason, the optical and infrared extinction has been used in several studies to infer the molecular gas column density in our MW (see Bohlin et al. 1978; Lada et al. 1994; Dobashi et al. 2005; Pineda et al. 2010). In external galaxies, Brinchmann et al. (2013) proposed a theoretical approach to use the extinction of the

* E-mail: a.concas@mrao.cam.ac.uk (AC)

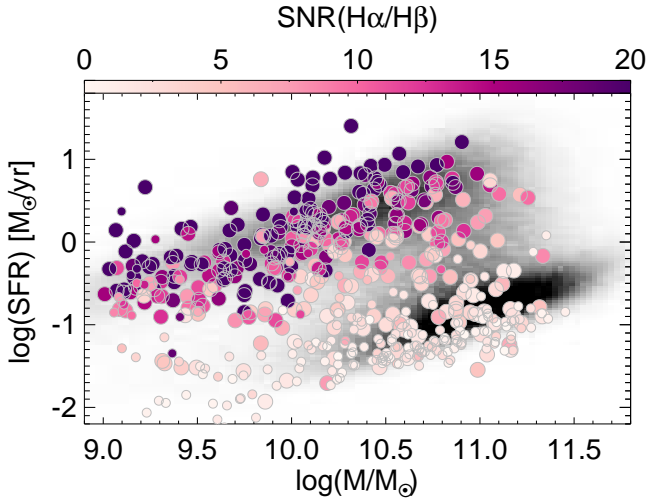


Figure 1. Distribution of the xCOLD GASS galaxy sample (big and small circles, for the CO detections and CO upper limits, respectively) in the SFR- M_* diagram, color-coded as a function of the Balmer Decrement signal-to-noise ratio, $\text{SNR}(\text{H}\alpha/\text{H}\beta)$. The gray-scale contours show the overall SDSS population. Our sample perfectly covers the entire region of star-forming galaxies in a wide range of M_* .

optical emission line fluxes in SDSS local galaxy spectra to indirectly constrain the dust and gas masses of the HII regions. The main limitation of this method is the nature of the fitting procedure that requires the a priori knowledge of the extinction law models, making the results necessarily model dependent (see Brinchmann et al. (2013) Section 3.2).

In this Letter, we investigate with an empirical approach whether the optical attenuation by dust, as seen by reddening of the Balmer lines ($\text{H}\alpha$ and $\text{H}\beta$), can be used as a proxy of the molecular gas mass by taking advantage of the largest CO survey ever conducted, the xCOLD GASS survey (see Saintonge et al. 2011, 2017). In particular, we study the correlation between BD estimated from the SDSS galaxy spectra, L_{CO} and M_{H_2} , provided for CO detected local xCOLD GASS galaxies.

In Section 2, we describe and characterize our galaxy sample. The L_{CO} -BD, M_{H_2} -BD and M_{HI} -BD correlations are presented in Section 3. Finally, we summarize our main conclusions in Section 4. Throughout this Letter, the following cosmological parameters are assumed: $H_0 = 70 \text{ km s}^{-1} \text{ Mpc}^{-1}$, $\Omega_M = 0.3$ and $\Omega_\Lambda = 0.7$.

2 DATA

2.1 The CO molecular gas mass and Balmer Decrement

The sample of galaxies analyzed in this work is taken from the extended CO Legacy Database for GASS survey (xCOLD GASS, Saintonge et al. 2017), designed to provide a picture of molecular gas across the local galaxy population. The sample consist of 532 galaxies observed at the IRAM 30 m telescope over the course of two large programs: the original COLD GASS survey (Saintonge et al. 2011) targeted 366 galaxies at $0.025 < z < 0.050$ with stellar

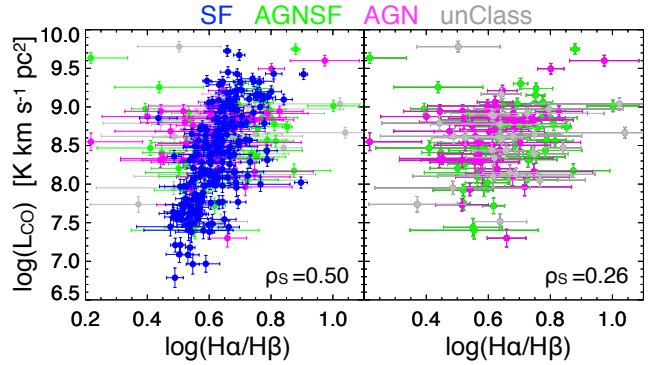


Figure 2. Left panel: L_{CO} versus $\text{H}\alpha/\text{H}\beta$ for a sample of 333 CO(1-0) detected xCOLD-GASS galaxies. The points are color-coded as a function of the BPT classification: SF systems (blue), composite SF and AGN systems (green), AGN (magenta), unclassifiable objects (low SNR emission lines, grey). Right panel: as in the left panel only for composite, AGN and unclassifiable systems. In both panels ρ_s indicates the value of the Spearman correlation coefficient.

mass $M_* > 10^{10} M_\odot$, and the subsequent COLD GASS-low survey (Saintonge et al. 2017), with 166 galaxies with $10^9 < M_* < 10^{10} M_\odot$ in a similar redshift range (Saintonge et al. 2017). The galaxies with detected CO line are 63% of the sample (333 objects), while for the remaining galaxies only L_{CO} and M_{H_2} upper limits are provided (see Saintonge et al. 2016, 2017).

For all galaxies in the xCOLD GASS sample the L_{CO} is converted to the total molecular gas mass, M_{H_2} by using the empirical relation: $M_{\text{H}_2} = \alpha_{\text{CO}} \times L_{\text{CO}}$, where α_{CO} is the CO-to- H_2 conversion factor (Dickman et al. 1986; Obreschkow & Rawlings 2009 and Kennicutt & Evans 2012 for a review) calibrated in Accurso et al. 2017.

The xCOLD GASS catalog also provides several global galaxy properties as: stellar mass (M_*), star formation rate (SFR), classification of the galaxies according to main ionization mechanism (star-forming, composite, AGN and unclassified galaxies according to the BPT diagram, Baldwin et al. 1981), galaxy size (r_{50} , the radius encapsulating 50% of the Petrosian r-band flux), gas-phase metallicity $12 + \log \text{O}/\text{H}$ (obtained from the $\text{N}[\text{II}]/\text{H}\alpha$ and $\text{O}[\text{III}]/\text{H}\beta$ ratio and the calibration of Pettini & Pagel 2004) and concentration index¹.

To retrieve an accurate value of the galaxy disk inclination we use the measures provided by the morphology catalogue of Simard et al. (2011) when available, and the xCOLD GASS sample otherwise. All the 532 xCOLD GASS galaxies are cross matched with SDSS DR7 MPA-JHU emission line catalog², which provides the measurements of $\text{H}\alpha$ and $\text{H}\beta$ fluxes and related uncertainties necessary to evaluate the Balmer Decrement (BD). As discussed on the MPA-JHU website, and well explained by Groves et al. (2012) and Brinchmann et al. (2013), the listed errors of the MPA/JHU catalogue are formal, and likely underestimated. Following

¹ $C_{\text{index}} = r_{90}/r_{50}$ is defined as the ratio of the r-band Petrosian radii encompassing 90% and 50% of the flux, which can be used as a proxy for the bulge-to-disk ratio, see e.g. Weinmann et al. 2009

² https://wwwmpa.mpa-garching.mpg.de/SDSS/DR7/raw_data.html

Table 1. L_{CO} -BD and M_{H_2} -BD best fit coefficients, for all the SF and the less inclined ($i \leq 65^\circ$) SF galaxy samples, obtained by using the prescription of Cappellari et al. 2013. σ , Δ_{obs} and N indicate the internal scatter, observed RMS of the residuals around the ordinate axis of the best-fit and the number of galaxies in each sub-sample, respectively.

	$\log L_{CO} = a \times (\log BD - x_0) + b$				$\log M_{H_2} = c \times (\log BD - x_0) + d$				
	a	b	σ	Δ_{obs}	c	d	σ	Δ_{obs}	N
SF	6.53 ± 0.44	8.33 ± 0.03	0.41 ± 0.03	0.46	5.59 ± 0.36	8.94 ± 0.03	0.30 ± 0.02	0.39	198
$i \leq 65^\circ$	8.52 ± 0.55	8.50 ± 0.04	0.33 ± 0.03	0.41	6.5 ± 0.46	9.07 ± 0.03	0.24 ± 0.03	0.35	127

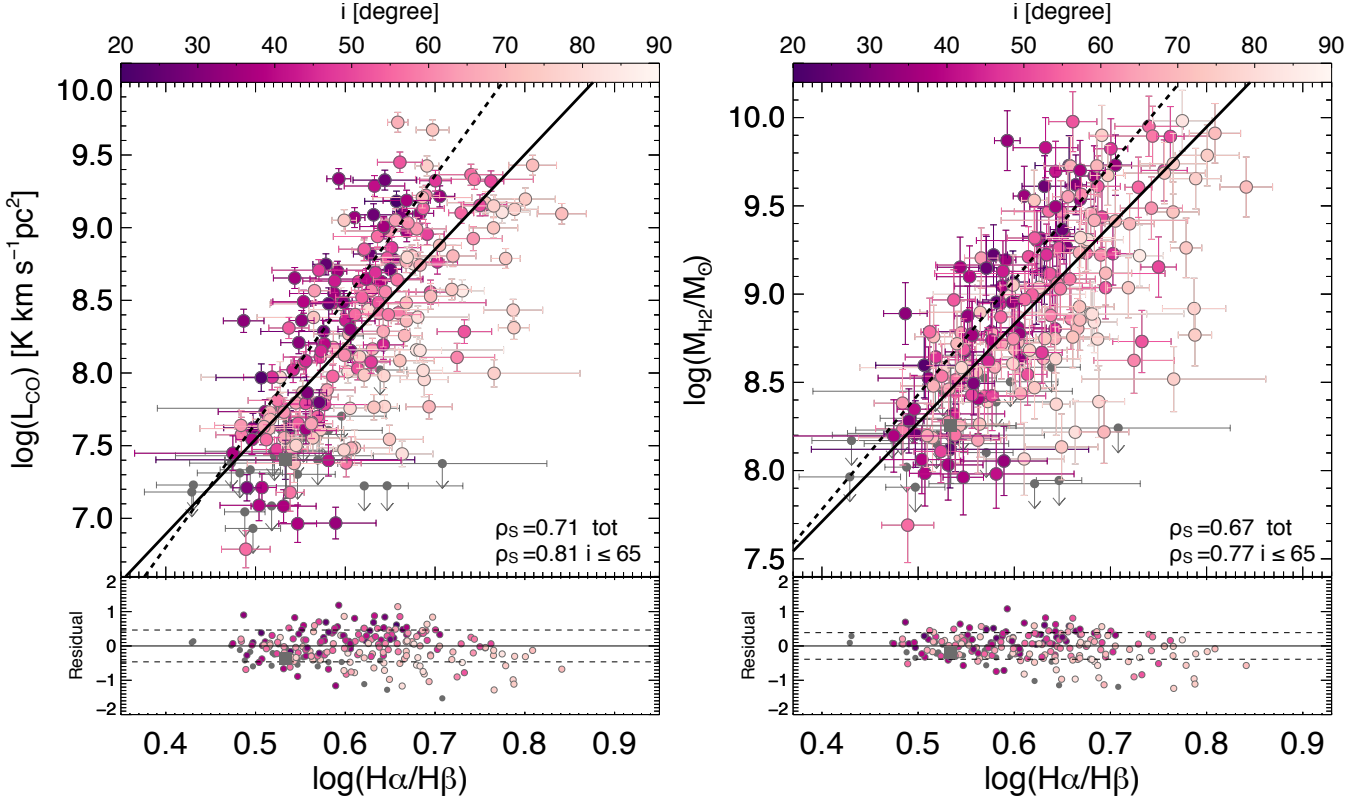


Figure 3. *Upper panels:* L_{CO} (left) and M_{H_2} (right) versus $H\alpha/H\beta$ for 222 SF xCOLD GASS galaxies, color-coded as a function of the disk inclination. L_{CO} luminosity upper limits and their average value are indicated with gray points and square, respectively. The best fit power law is shown for the whole sample (solid line) and for the subsample at low disk inclination ($i \leq 65^\circ$, dashed line). The Spearman coefficient, ρ_S , is reported in both panels for the whole sample and the low inclination subsample. *Lower panels:* residuals as a function of $H\alpha/H\beta$ with respect to the best fit power law obtained for the whole sample.

the approach of Brinchmann and collaborators, we multiplied the uncertainty of the emission lines by a correction factor ($f = 2.473$ and $f = 1.882$ for the $H\alpha$ and $H\beta$ line respectively), to take into account continuum subtraction errors.

All xCOLD GASS galaxies have a match in the MPA/JHU catalogue and so a measure of the BD. In Fig. 1 we illustrate the distribution of our sample in the SFR- M_* plane. The points are color-coded as a function of the BD signal-to-noise-ratio, $SNR(H\alpha/H\beta)$. As expected, the BD is well detected in galaxies on and above the Main Sequence (MS) of star forming galaxies but it shows a progressively lower SNR at larger distances from the MS towards the quiescence region. Finally, by cross matching the xCOLD GASS sample with the xGASS sample provided by Catinella et al. (2018) we obtained a subsample of 253, with a estimate of atomic gas mass (M_{HI}), M_{H_2} and BD.

3 THE BALMER DECREMENT- L_{CO} AND M_{H_2} CORRELATION

First, we study the correlation between the luminosities of the CO(1-0) line, L_{CO} , versus the Balmer decrement, (BD= $H\alpha/H\beta$) in the xCOLD GASS subsample with a detected CO(1-0) emission (333 galaxies). The correlation is significant when the whole subsample is considered, with a Spearman rank coefficient (Spearman 1904) ρ_S of 0.5 and a 99% probability of correlation (left panel of Fig.2). The significance of the correlation increases substantially ($\rho_S = 0.71$) and the scatter decreases when only pure SF galaxies are considered. Instead, unclassified, composite SF/AGN and AGN dominated galaxies exhibit a much larger scatter and a poor correlation ($\rho_S = 0.26$, right panel of Fig.2). Such lack of correlation in the non SF galaxies is not surprising. Indeed, unclassified galaxies tend to be located in the quiescence region, where the BD SNR is poor (1). In addition,

Table 2. L_{CO} -BD-i and M_{H_2} -BD-i best fit coefficients, for all the SF galaxies, obtained by using the prescription of Cappellari et al. 2013. σ , Δ_{obs} and N indicate the internal scatter, observed RMS of the residuals around the ordinate axis of the best-fit and the number of galaxies, respectively.

	$\log L_{CO} = a + b \times (\log BD - \log BD_0) + c \times (i - i_0)$				$\log M_{H_2} = d + f \times (\log BD - \log BD_0) + g \times (i - i_0)$						
	a	b	c	σ	Δ_{obs}	d	f	g	σ	Δ_{obs}	N
SF	8.32 ± 0.03	7.59 ± 0.43	-0.013 ± 0.002	0.36 ± 0.03	0.43	8.93 ± 0.03	5.86 ± 0.35	-0.010 ± 0.002	0.26 ± 0.03	0.36	198

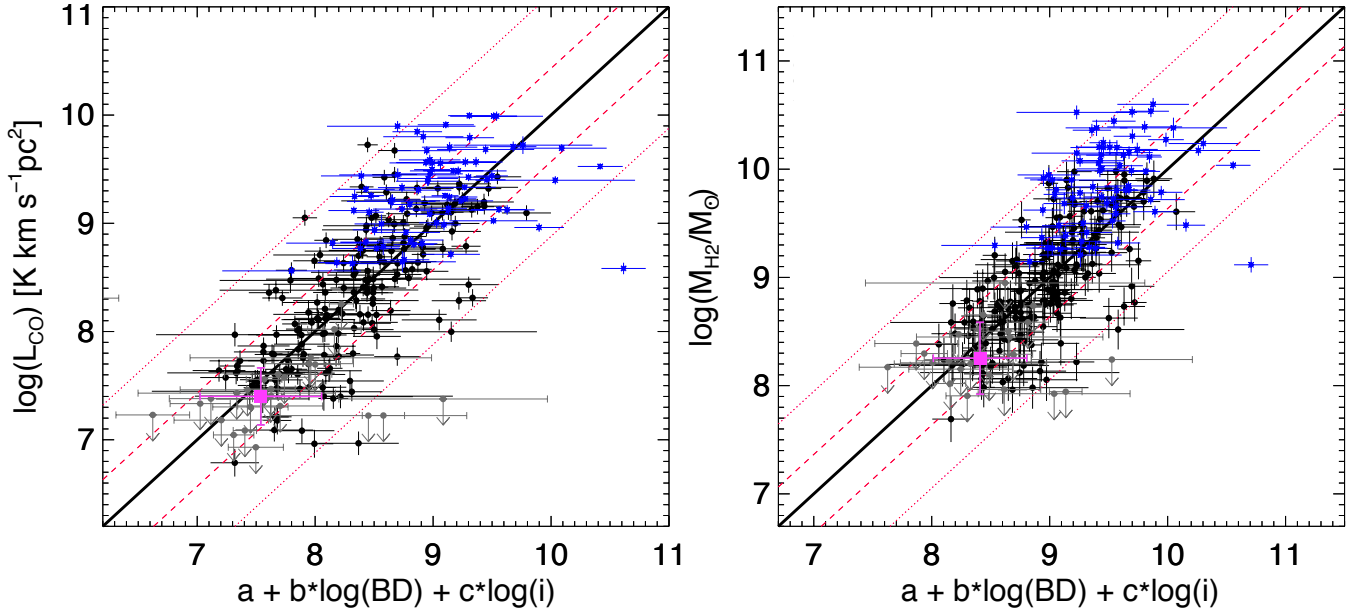


Figure 4. L_{CO} and M_{H_2} versus $H\alpha/H\beta$ (BD) corrected for the disk inclination (i) for for the same sample as in Fig. 3. Upper limits are indicated by gray points. The magenta square is the average value of the upper limits. The red lines mark the 1σ (dashed) and 2.6σ (dotted) regions. The errors bars are the projection of the observational errors. The blue stars represent the 78 starburst galaxies taken from the Bertemes et al. (2018) catalogue.

in AGN hosts and composite systems the optical emission is probably affected by the photons originated in the narrow line regions which are not directly connected with the presence of cold molecular gas.

We limit the study of the correlation to the 226 pure SF galaxies, of which 201 galaxies with detected CO(1-0) emission and 25 L_{CO} upper limits. To avoid spurious results due to the presence of galaxies with complex morphology (merging like systems) and/or uncorrected BD measurement, we remove 4 object from the SF sample. The final SF sample consist of 222 SF galaxies, 198 with detected CO emission and 24 upper limits (see Fig. 3). The data are fitted with a power law of the form: $\log L_{CO} = a \times (\log BD - x_0) + b$ by using the LTS_LINEFIT code presented by Cappellari et al. (2013), which allows for errors in both variables and intrinsic scatter (defined as the dispersion of the data along the y-direction due to the physical values rather than to measurement errors, see Tremaine et al. 2002; Cappellari et al. 2013 for more details). To minimize the uncertainty on the intercept (b), we use a reference value close to the middle of the x values, $x_0 = 0.62$. The best fit power law is showed in Fig. 3, left panel. The best fit coefficients, internal scatter and observed RMS along the y-coordinate are reported in Tab. 1, left part. The fitting procedure does not include the L_{CO} upper limits. However, we point out that such upper

limits and their mean value (grey symbols, in left panel of Fig. 3) follow the average trend.

By adopting a constant conversion factor (e.g. $\alpha_{CO}^{MW} = 4.3 M_{\odot}/K \text{ km s}^{-1} \text{ pc}^2$ for the Milky Way, see the discussion in Bolatto et al. 2013) this correlation can be easily translated to a M_{H_2} -BD correlation of the form: $\log L_{CO} + \log \alpha_{CO}^{MW} = \log M_{H_2}$. Differently, if a non-constant conversion factor is assumed, the shape of the relation could be different. As an example, in the right panel of Fig. 3 we report the molecular mass, M_{H_2} -BD relation obtained by using the M_{H_2} obtained with the α_{CO} proposed by Accurso et al. 2017, witch depends primarily on gas metallicity and secondarily on the offset from the star-forming main sequence.

In order to understand what are the possible sources of scatter we first study our L_{CO} -BD and M_{H_2} -BD correlations against the galactic disk inclination. As expected, systems with the highest inclination tend to exhibit extremely high values of the BD compared to the less inclined galaxies (as shown by the colour coding on Fig. 3). This is likely due to the fact that in edge-on systems, the $H\alpha$ and $H\beta$ photons need to pass through the entire disk before escaping the galaxy, with a large probability of being absorbed by the disk itself. The disk self-obscuration leads to large values of BD with respect to the actual amount of dust that is linked to the molecular clouds.

To take into account this effect, we test two different

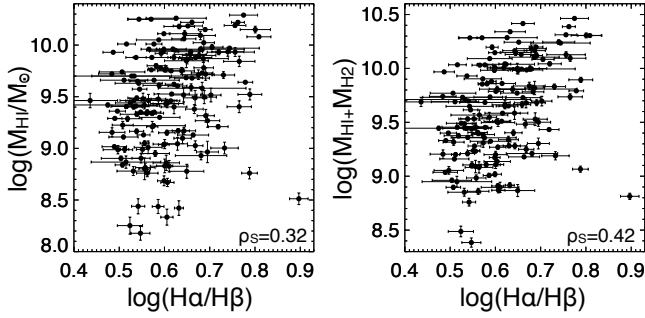


Figure 5. M_{HI} (left) and total gas mass ($M_{H2}+M_{HI}$, right) versus $H\alpha/H\beta$ for 158 SF galaxies with molecular and atomic estimates. The Spearman correlation coefficient ρ_S is indicated in both panels. The errors in the atomic mass are evaluated by taking into account the errors in the HI flux.

approaches. First, we reduce our sample on galaxies with $i \leq 65^\circ$. In this case, the Spearman correlation coefficient increases in both L_{CO} -BD and M_{H2} -BD correlations. Similarly the intrinsic and the observed scatter decreases respectively to ~ 0.3 and ~ 0.4 dex in L_{CO} and to ~ 0.24 and ~ 0.4 dex in M_{H2} case. The fit parameters are reported on Tab. 1. As an alternative approach, we parametrize the L_{CO} as a function of BD and the galaxy inclination using the plane fitting prescription proposed by Cappellari et al. (2013): $\log L_{CO} = a + b \times (\log BD - \log BD_0) + c \times (i - i_0)$, where $\log BD_0 = 0.62$ and $i_0 = 56^\circ$ are the adopted reference values. We use the same form for the M_{H2} -BD relation. The best fit values are reported in Tab.2 for both the L_{CO} and M_{H2} . Also in this case, the correlations are tighter, with a reduction of the intrinsic and observed scatter of 0.36 ± 0.03 and 0.43 dex in L_{CO} and 0.26 ± 0.03 and 0.36 dex on the M_{H2} case.

As reported from several previous studies, the gas-to-dust ratio clearly depends on gas metallicity (e.g. Draine et al. 2007; Galametz et al. 2011). However, we notice that our correlation is stable across our gas metallicity range, $8.45 < 12 + \log OH < 8.8$. To test the L_{CO} -BD and the L_{CO} -BD- i correlations against biases, we study the distribution of the residuals against several parameters such as the galaxy size, concentration index, stellar mass and SFR. No correlations are observed in both the L_{CO} -BD and the L_{CO} -BD- i case, between the residuals and the other parameters considered, as confirmed by the Spearman test.

Finally, to test the reliability of the correlation, we overplot in Fig. 4 the *Herschel* SPIRE selected sample of Bertemes et al. (2018) in the SDSS Stripe82 area. The shallow *Herschel* Stripe82 survey leads to the selection of the dustiest local objects. Bertemes et al. (2018) provide a measure of L_{CO} for a subsample of WISE and SPIRE simultaneously detected systems with Alma CO follow-up. Such objects, which sample the highest L_{CO} and M_{H2} end, remarkably follow the correlation given by the xCOLD GASS sample.

4 THE BALMER DECREMENT- M_{HI} CORRELATION

For a subsample of 158 SF galaxies with both atomic and molecular mass, we consider also the relation between

Balmer decrement and atomic gas mass (M_{HI}) taken from the xGASS catalogue (see Catinella et al. 2018). First, one should consider that the molecular mass itself does not correlate significantly with the HI gas mass, as found in Catinella et al. (2013, 2018). This is due to the fact that the molecular gas mass is located mainly in the star forming region of the galaxy stellar disk, while the HI disk is much more extended (Catinella et al. 2018). Similarly the BD does not correlate strongly with the HI mass as shown in the left panel of Fig. 5. In the same way, the total cold gas mass, given by the sum of the HI and H2 gas mass, shows only a poorly significant correlation with the BD (right panel of Fig. 5), as the atomic phase is dominating over the molecular gas.

5 CONCLUSIONS

We find a tight correlation between the dust screen surrounding the HII regions, traced by the Balmer Decrement (BD) and the cold molecular gas (M_{H2}) traced by the CO(1-0) luminosity (L_{CO}) in a sample of 222 local star-forming galaxies taken from the xCOLD GASS survey. In AGN, composite and unclassified galaxies the correlation is not visible due to the contamination by the nuclear region or the very low SNR of the Balmer emission lines.

As expected, the galaxy inclination leads to the observation of extremely high value of BD in edge-on galaxies. Once corrected for the disk self-obscuration in such highly inclined galaxies, the BD can be used as a very powerful proxy of the L_{CO} and the M_{H2} in local star forming galaxies, with a scatter of ~ 0.3 dex. We test the correlation against possible biases induced by the physical properties of our sample, as the galaxy size, mass, morphology, star formation activity and gas metallicity but we do not find any dependence of the residuals on the considered parameters. The retrieved relation also matches the L_{CO} -BD distribution of the dustiest local objects, identified in the *Herschel* Stripe82 survey (Bertemes et al. 2018). We highlight the fact that our relation is calibrated on local massive ($M_\star > 10^9 M_\odot$) and metal rich galaxies ($12 + \log OH > 8.45$), any future application outside of its range of validity should be taken with caution. We do not find a significant correlation if the atomic gas phase is taken into account. This is likely due to the fact that the region traced by the BD, the stellar disk, is much smaller than the HI disk.

ACKNOWLEDGEMENTS

AC thanks Federico Lelli for precious suggestions and stimulating discussion. AC is grateful to Luca Cortese, Roberto Maiolino and Asa F. L. Bluck for the interesting suggestions and Barbara Catinella for the clarification concerning the COLD GASS dataset. This research was supported by the DFG cluster of excellence "Origin and Structure of the Universe". The authors acknowledge all the members of the xCOLD GASS (Saintonge et al. 2011, 2017) and COLD GASS (Catinella et al. 2010, 2018) projects for providing the data.

REFERENCES

- Accurso G., et al., 2017, *MNRAS*, **470**, 4750
- Baldwin J. A., Phillips M. M., Terlevich R., 1981, *PASP*, **93**, 5
- Barrera-Ballesteros J. K., et al., 2018, *ApJ*, **852**, 74
- Bertemes C., et al., 2018, *MNRAS*, **478**, 1442
- Bohlin R. C., Savage B. D., Drake J. F., 1978, *ApJ*, **224**, 132
- Bolatto A. D., 2015, in *EAS Publications Series*. pp 81–86
([arXiv:1512.02269](https://arxiv.org/abs/1512.02269)), doi:10.1051/eas/1575014
- Bolatto A. D., Wolfire M., Leroy A. K., 2013, *ARA&A*, **51**, 207
- Boquien M., et al., 2013a, *A&A*, **554**, A14
- Boquien M., et al., 2013b, *A&A*, **554**, A14
- Bourne N., et al., 2013, *MNRAS*, **436**, 479
- Brinchmann J., Charlot S., Kauffmann G., Heckman T., White S. D. M., Tremonti C., 2013, *MNRAS*, **432**, 2112
- Calzetti D., Kinney A. L., Storchi-Bergmann T., 1994, *ApJ*, **429**, 582
- Cappellari M., et al., 2013, *MNRAS*, **432**, 1709
- Catinella B., et al., 2010, *MNRAS*, **403**, 683
- Catinella B., et al., 2013, *MNRAS*, **436**, 34
- Catinella B., et al., 2018, *MNRAS*, **476**, 875
- Charlot S., Fall S. M., 2000, *ApJ*, **539**, 718
- Dame T. M., Hartmann D., Thaddeus P., 2001, *ApJ*, **547**, 792
- Dickman R. L., Snell R. L., Schloerb F. P., 1986, *ApJ*, **309**, 326
- Dobashi K., Uehara H., Kandori R., Sakurai T., Kaiden M., Umemoto T., Sato F., 2005, *PASJ*, **57**, S1
- Draine B. T., et al., 2007, *ApJ*, **663**, 866
- Eales S. A., et al., 2010, *A&A*, **518**, L62
- Eales S., et al., 2012, *ApJ*, **761**, 168
- Galametz M., Madden S. C., Galliano F., Hony S., Bendo G. J., Sauvage M., 2011, *A&A*, **532**, A56
- Groves B., Brinchmann J., Walcher C. J., 2012, *MNRAS*, **419**, 1402
- Groves B. A., et al., 2015, *ApJ*, **799**, 96
- Israel F. P., 1997, *A&A*, **317**, 65
- Israel F. P., 2005, *A&A*, **438**, 855
- Israel F. P., Bontekoe T. R., Kester D. J. M., 1996, *A&A*, **308**, 723
- James A., Dunne L., Eales S., Edmunds M. G., 2002, *MNRAS*, **335**, 753
- Kennicutt R. C., Evans N. J., 2012, *ARA&A*, **50**, 531
- Kreckel K., et al., 2013, *ApJ*, **771**, 62
- Lada C. J., Lada E. A., Clemens D. P., Bally J., 1994, *ApJ*, **429**, 694
- Leroy A. K., et al., 2009, *ApJ*, **702**, 352
- Obreschkow D., Rawlings S., 2009, *MNRAS*, **394**, 1857
- Pettini M., Pagel B. E. J., 2004, *MNRAS*, **348**, L59
- Pineda J. L., Goldsmith P. F., Chapman N., Snell R. L., Li D., Cambr esy L., Brunt C., 2010, *ApJ*, **721**, 686
- Roman-Duval J., et al., 2010, *A&A*, **518**, L74
- Saintonge A., et al., 2011, *MNRAS*, **415**, 32
- Saintonge A., et al., 2016, *MNRAS*, **462**, 1749
- Saintonge A., et al., 2017, *ApJS*, **233**, 22
- Scoville N., et al., 2014, *ApJ*, **783**, 84
- Scoville N., et al., 2015, preprint, ([arXiv:1505.02159](https://arxiv.org/abs/1505.02159))
- Scoville N., et al., 2016, *ApJ*, **820**, 83
- Scoville N., et al., 2017, *ApJ*, **837**, 150
- Simard L., Mendel J. T., Patton D. R., Ellison S. L., McConnachie A. W., 2011, *ApJS*, **196**, 11
- Spearman C., 1904, *The American Journal of Psychology*, **15**, 72
- Tremaine S., et al., 2002, *ApJ*, **574**, 740
- Weinmann S. M., Kauffmann G., van den Bosch F. C., Pasquali A., McIntosh D. H., Mo H., Yang X., Guo Y., 2009, *MNRAS*, **394**, 1213
- Wolfire M. G., Hollenbach D., McKee C. F., Tielens A. G. G. M., Bakes E. L. O., 1995, *ApJ*, **443**, 152

This paper has been typeset from a $\text{\TeX}/\text{\LaTeX}$ file prepared by the author.